

# Self-Packaging and Self-Mounting of Miniaturized Semiconductor Dies Across Length Scales and 3D Topologies

Robert J. Knuesel, Se-Chul Park, and Heiko O. Jacobs  
Department of Electrical and Computer Engineering, University of Minnesota,  
200 Union Street SE, Minneapolis, Minnesota 55455

## ABSTRACT

This proceeding reviews recent progress in fluidic surface-tension-directed self-assembly involving liquid solder which has been applied to the self-packaging and self-mounting of discrete inorganic semiconductor device components at different length scales producing electrically interconnected devices and systems. Results included flip chip self-assembly with unique angular orientation and contact pad registration, parallel packaging and encapsulation, and the programmable self-mounting of various types of components ranging from phototransistors, to LEDs, to photovoltaic cells. We discuss recent challenges in extending the minimal component size below the 100  $\mu\text{m}$  barrier where prior component delivery and agitation concepts have not worked. A new delivery system is presented to concentrate and effectively introduce the components which involves a liquid-liquid interface and energy cascade that drives the assembly process forward yielding a conveyor like assembly process. Recent applications include the tiling of curved and 3D surfaces with tiles of single crystal Si forming curved and 3D solar cells on plastic substrates.

## INTRODUCTION

The construction of man-made artifacts such as cell phones and computers relies on robotic assembly lines that place, package, and interconnect a variety of devices that have macroscopic ( $>1$  mm) dimensions<sup>[1]</sup>. The key to the realization of these systems is our ability to integrate/assemble components in 2D/3D as well as link/interconnect the components to transport materials, energy, and information. The majority of these systems that are on the market today are heterogeneous in nature. Heterogeneous systems can be characterized as systems that contain at least two separate parts, thereby prohibiting monolithic integration. Such systems are typically fabricated using robotic pick and place. The size of the existing systems could be reduced by orders of magnitudes if microscopic building blocks could be assembled and interconnected effectively<sup>[2]</sup>. The difficulty is not the fabrication of smaller parts, but their assembly into an interconnected system. For components with dimensions less than 100  $\mu\text{m}$ , adhesive capillary forces often dominate gravitational forces, making it difficult to release the components from a robotic manipulator<sup>[3]</sup>. As a direct result, heterogeneous integration using an extension of serial robotic pick and place and wire-bonding has not proven a viable solution.

At the other extreme, nature forms materials, structures, and living systems by self-assembly on a molecular length scale<sup>[4,5]</sup>. As a result, self-assembly based fabrication strategies are widely recognized as inevitable tools in nanotechnology and an increasing number of studies are being carried out to “scale-up” these concepts to close the assembly gap between nanoscopic and macroscopic systems. Recent demonstrations of processes that can assemble micrometer to millimeter-sized components include: shape-directed fluidic methods that

assemble trapezoidal parts on planar surfaces on the basis of gravity and complementary 3D shapes [6, 7], liquid-solder-based self-assembly that uses the surface tension between pairs of molten solder drops to assemble functional systems [8-10], capillary force-directed self-assembly that uses hydrophilic/hydrophobic surface patterns and photo-curable polymers to integrate micro-optical components, micro-mirrors and semiconductor chips on silicon substrates [11-13], and sequential shape-and-solder-directed self-assembly that combines 3D shapes to define a chaperone with solder directed assembly to effectively assemble electrically interconnected parts [14-19]. The sequential shape-and-solder-directed self-assembly process has been applied to flip-chip assembly with unique contact pad registration [16] as well as the packaging of light emitting diodes [14-16] and transponders that can be interrogated remotely [17]. Comparing more recent concepts [18, 19] with the pioneering work by Yeh and Smith [6, 7], there are a number of fundamental differences: Recent methods do not require trapezoidal chips to prevent upside down assembly and asymmetric L or T shaped chip designs for angular orientation control. Instead they use simple shapes or openings in combination with solder coated areas to enable assembly in 3D or in 2D considering flip-chip assembly with unique angular orientation and contact pad registration. The openings are bigger than the components and act as guides for the solder directed self-assembly process. The solder drives the assembly into the aligned stable position and the driving force is surface tension, as opposed to gravity. Recent studies have also overcome the difficulty in assembling more than one component type through sequential methods that either use activation of selected receptors [20] or different sized openings [14-16]. Unique orientation no longer requires asymmetric three dimensional chips including triangular, L or T shaped parts that are not very common. While a number of applications have been demonstrated, scalability to smaller dimensions remains a challenge. Stauth et al. has successfully tested shape and solder directed self-assembly with 100  $\mu\text{m}$  sized components [21], which are three times smaller than our previously reported parts [16]. This paper extends prior work [10, 14-16] in the area of shape and solder directed self-assembly to smaller scales. It reports on angular orientation control, flip-chip assembly, and recent progress in the assembly of ultra small chiplets with a side length of 20  $\mu\text{m}$ . A new system employing a liquid-liquid interface will be presented to deliver and concentrate components with correct pre-orientation.

**Figure 1**  
*Self-assembly of dies using A) solder-based alignment alone, B) wells for size discrimination, and C) combined pedestals -, solder -, and IO - layouts that supports single-angle orientation and flip-chip contact pad registration.*

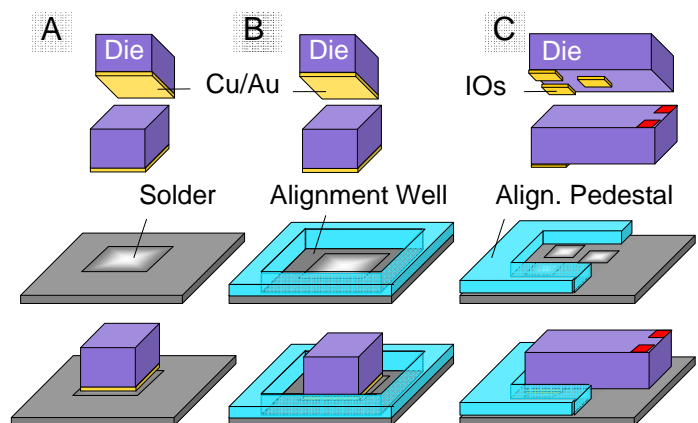
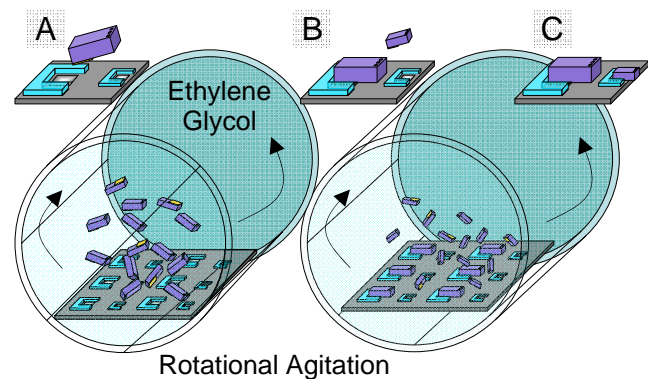


Figure 1 illustrates the basic concept of solder directed self-assembly (Figure 1A) introducing alignment pedestals and contact pad layouts with increasing complexity. The layout shown in Figure 1B prevents assembly of more than one component type onto a single receptor, while the layout in Figure 1C enables flip-chip assembly with single-angle orientation and contact pad registration forming multiple contacts to the device: Components can only attach to the solder-coated areas if a correct angular pre-orientation condition is met. Components that arrive at the docking sites with an angular orientation that deviates by more than  $\pm 90^\circ$  from the desired orientation will not find a sufficient overlap between the binding site (contact area) on the components and the solder-coated areas and therefore will not attach. Other components will be captured and aligned due to the reduction of the interfacial free energy.

## EXPERIMENTS WITH COMPONENTS 300 $\mu\text{m}$ – 3 mm IN SIZE

Figure 2 shows the sequential self-assembly procedure that we employ to batch-assemble differently sized components with a single-angle orientation. Following the large component assembly in Figure 2A, small components are assembled as in Figure 2B with complete differently sized component assembly shown in Figure 2C. When assembled in this order, large components will not assemble on the small docking sites due to the chaperone, while small components will be blocked from assembling on large docking sites by the previously assembled large sites. The assembly was performed in a glass vial that was filled with ethylene glycol at a temperature of 150  $^\circ\text{C}$  so the solder was molten. Ethylene glycol was used to accommodate the higher melting point solder that is not compatible with a water-based assembly solution. We used both a low- (47  $^\circ\text{C}$ ) and medium- (138  $^\circ\text{C}$ ) melting-point (mp) solders (Y-LMA-117 and LMA-281, Small Parts, Miami Lakes, FL) in our experiments; we did not observe a notable difference between the two. The ethylene glycol solution was made slightly acidic (pH  $\sim 4.0$ ) with hydrochloric acid to remove metal oxide from the surface of the solder drop; an oxide layer that — if sufficiently thick — blocked the wetting of the metal surface. Component transport and mixing was provided by hand agitation of the vial/drum to accomplish a tumbling motion across the surface, a motion that needs to be automated in future work.

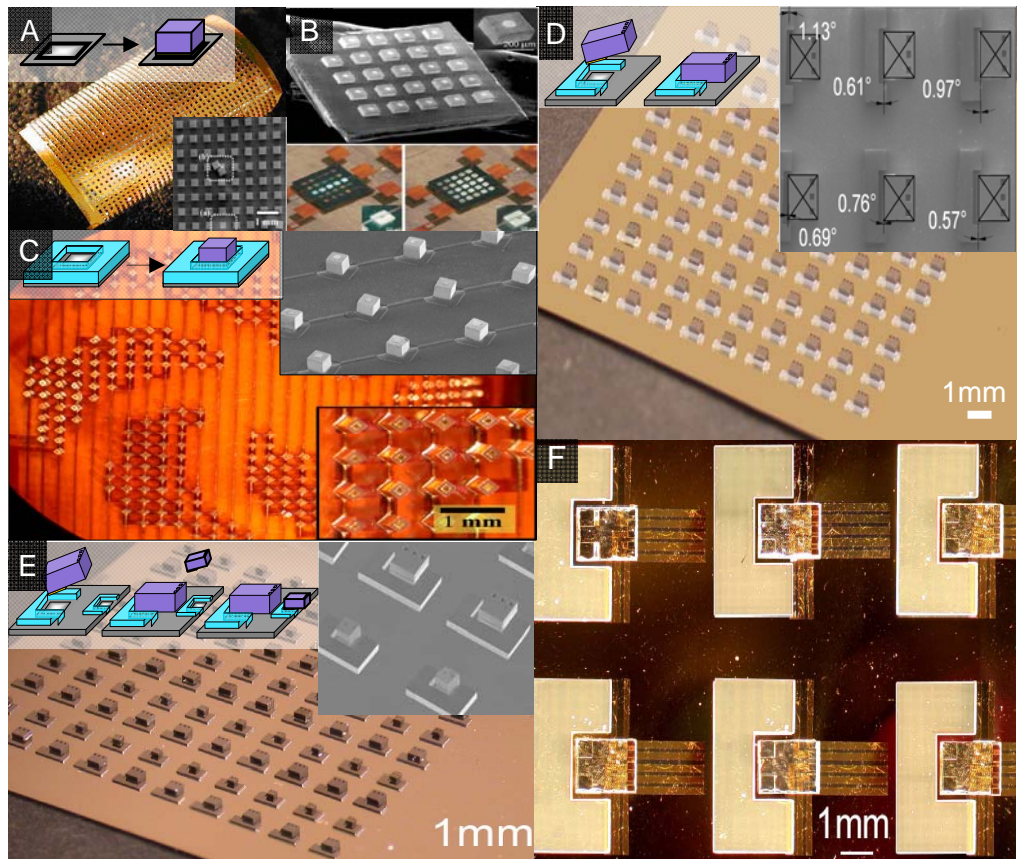


**Figure 2**  
*Rotational agitation procedure showing a two-step process to integrate multiple types of chiplets on a single substrate.*

Through the course of this study we tested a number of different components including GaAlAs-LEDs, Si, glass, and SU-8 blocks with different pad layouts. Figure 3 represents a summary of the results. Figure 3A illustrates 1500 silicon chiplets, 300  $\mu\text{m}$  on a side, which assembled onto a flexible polyimide surface with 98% coverage. With  $\sim 5000$  components inside

the vials, the assembly took about 90 s to reach steady state and was completed in 3 minutes. The lateral and angular precision was  $\sim 15 \mu\text{m}$  and  $\sim 3^\circ$ , respectively, and limited by non-uniformity of the components that were fabricated by dicing using a dicing saw. Figure 3B shows GaAs/GaAlAs light-emitting diodes that have been assembled on a silicon substrate. The insets show the LEDs under operation. Without alignment pedestals, two chiplets can occupy a single receptor which is considered a defect. This defect can be eliminated using alignment pedestals as illustrated in Figure 3C. The entire assembly contained 196 interconnected LEDs with a side length of  $280 \mu\text{m}$ . The chiplets assembled with four stable orientations  $0^\circ$ ,  $90^\circ$ ,  $180^\circ$ , and  $270^\circ$ . Figure 3D introduces unique angle orientation self assembly to reduce the number of stable orientations to one. A single-type component  $10 \times 10$  array was assembled to determine alignment accuracy. The resulting accuracy of the self-assembly process was determined using the standard deviation which was  $0.3^\circ$  for the angular orientation and  $19 \mu\text{m}$  for lateral accuracy. Figure 3E is an example of sequential batch assembly showing a  $10 \times 10$  array that contains  $900 \mu\text{m}$  and  $500 \mu\text{m}$  sized dies assembled using a two-step self-assembly sequence. The largest components were  $2 \times 1 \times 1 \text{ mm}$  glass blocks. The blocks assembled with unique orientation and attached to 7 contacts on the substrate that are visible from the top (Figure 3F). The smallest components were  $280 \mu\text{m}$  on a side (Figure 3C).

**Figure 3**  
 Summary of self-assembly results with varying docking site types using AlGaAs-LEDs, Si, Glass, and SU-8 blocks. A) Simple solder-directed assembly of silicon parts, B) simple solder-directed assembly of LEDs, C) well assembly, D) unique-angle orientation assembly, E) sequential batch assembly using “two-step” docking sites, and F) flip-chip assembly of parts with multiple IO connections.



## EXPERIMENTS WITH COMPONENTS 20 – 100 μm IN SIZE

It should be possible to scale down solder directed self-assembly to handle much smaller components than what has been demonstrated in Figure 3. The surface free energy of liquid solder dominates thermal energy and Brownian motion down to the sub-1 μm scale. In practice, however, scaling has been challenging. The problem is a surface oxide that forms due to residual oxygen, blocking the self-assembly. To combat this problem, small amounts of acid are added (pH 2-4) to the assembly solution. The acid addition, however, leads to an oxidative dissolution of the solder, an issue which becomes increasingly important as the solder volume is reduced. There are a number of potential solutions to this problem. In this study we present a new component delivery mechanism to speed up the self-assembly process. The new surface tension directed self-assembly approach [22] eliminates the dependency on gravity and sedimentation that becomes increasingly ineffective in delivering highly scaled (< 100 μm) components to the substrate. Instead, the method uses a liquid-liquid-solid interface to define a progressing linear front for the self-assembly to take place in a conveyor belt-like fashion.

Figure 4 illustrates the experimental strategy of surface tension directed self-assembly of ultra small dies at a liquid-liquid-solid interface [22]. The process uses a stepwise reduction of the interfacial energy to (i) move components from a suspension to the interface (55 mJ/m<sup>2</sup>), (ii) pre-orient the components within the interface to face in the right direction (90 mJ/m<sup>2</sup>), and (iii) assemble the components on molten solder through dipping (400 mJ/m<sup>2</sup>). To achieve this energy cascade it is necessary to correctly choose and/or adjust the surface energies. We tested a water-oil interface and components made out of SU-8 and silicon (20 μm wide, 20 μm deep, 10 μm thick and 60 μm wide, 60 μm deep, 20 μm thick, respectively) with a gold coated contact on one face. The gold surface was treated with a mercaptoundecanoic acid (MUA) self assembled monolayer (SAM) in a 10 mM (ethanol) solution for 15 minutes to render it hydrophilic, while the silicon faces were treated to become hydrophobic using 3-glycidoxypyltrimethoxysilane (GPTMS, Dow Corning Z-6040) by soaking with 200 mM GPTMS in ethanol for 15 minutes followed by a dehydration bake at 115°C for 5 minutes. The SU-8 surface was hydrophobic and needed no adjustments. These treatments yield the measured tabulated (Fig 4, bottom) contact angles and interfacial energies between the solids and liquids as determined using Young's equation  $\gamma_{s,l} = \gamma_s - \gamma_l \cos(\theta_{s,l})$  (29) where  $\gamma_s$  (usually not known) is the surface energy of the solid,  $\gamma_l$  (known) is the surface energy of the liquid, and  $\theta_{s,l}$  is the measured contact angle (known). The surface energy of water, silicone oil, and solder (Y-LMA-117, mp. 47°C, Small Parts, Miami Lakes, Florida) are 72, 20, ~500 mJ/m<sup>2</sup>, respectively, at a temperature of 95 °C where the solder is molten. The surface energies of the solids  $\gamma_s$  (typically unknown) are not needed as this parameter cancels out when computing the energy differences. For example, considering the illustrated cubic component, the transition from being immersed in oil to the interface is favored because the hydrophilic gold surface prefers to be in contact with water instead of oil; transfer to the liquid-liquid interface is favored by  $55 \text{ mJ/m}^2 = \gamma_{\text{Au,water}} - \gamma_{\text{Au,oil}} = \gamma_{\text{oil}} \cos(\theta_{\text{Au,oil}}) - \gamma_{\text{water}} \cos(\theta_{\text{Au,water}})$ . The components are confined to this interface since they face a  $35 \text{ mJ/m}^2 = (\gamma_{\text{Si,oil}} - \gamma_{\text{Si,water}}) * 5 = (\gamma_{\text{water}} \cos(\theta_{\text{Si,water}}) - \gamma_{\text{oil}} \cos(\theta_{\text{Si,oil}})) * 5$  energy barrier preventing them from completely entering the water because the 5 hydrophobic Si sides prefer to remain in contact with oil instead of water. For a cube to be oriented upside down within the interface would require the sum of 90 mJ/m<sup>2</sup>. Consequently, the components are introduced to the solder with the correct orientation whereby the gold side faces the solder with a water layer in between.



Solder has a higher affinity to wet the gold contact than water and attachment is favored by  $400 \text{ mJ/m}^2$ .

The actual transfer and self-assembly onto the substrate occurs as the sample is pulled upward through the interface (Fig. 4). Upward motion at a typical speed of  $30 \text{ mm/s}$  reduces the contact angle forming a receding water layer that becomes sufficiently thin for the gold to contact the solder. Transfer onto the solder-coated substrate occurs within this thin progressing interface in a conveyor belt-like fashion. For the assembly to work well the following conditions were essential. The temperature has to be maintained constant, which is achieved using a heated ethylene glycol bath that is kept at  $95 \text{ }^\circ\text{C}$  surrounding the glass assembly container. Metal surfaces including the solder need to be free of surface oxide which is achieved by reducing the pH of the assembly solution to pH 2.0 by adding drops of hydrochloric acid. It is possible to get good  $> 90\%$  coverage in a single pass; however, full coverage ( $99\%-100\%$ ) required several passes through the interface. Assembly in this system occurs only during upward motion. Downward motion removes loose unassembled components which transition back to the liquid-liquid interface. Saturation is observed in 5-10 passes which takes less than 1 minute.

**Fig. 4.** Procedure of surface tension directed self-assembly at a liquid-liquid-solid interface employing an energy cascade to (i) move components from a suspension to the interface ( $55 \text{ mJ/m}^2$ ), (ii) pre-orient the components within the interface to face in the right direction ( $90 \text{ mJ/m}^2$ ), and (iii) assemble the components on molten solder through dipping ( $400 \text{ mJ/m}^2$ ). The illustration depicts the situation for an oil-water interface and chiplets made out of Si which carry an Au contact on one face. Depicted Au and Si surfaces are treated using hydrophilic MUA and hydrophobic GPTMS functional groups and yield the tabulated measured contact angles, calculated solid-liquid-interfacial-energies, and energy differences (gray boxes to the right) required to drive the assembly. The available area and curved shape of the interface cause the components to form a closely packed 2D sheet. Upward motion of substrate yields a dynamic contact angle where the receding water layer becomes sufficiently thin for the gold to contact the solder. Patterned assembly on solder is favored by  $400 \text{ mJ/m}^2$  within this layer.

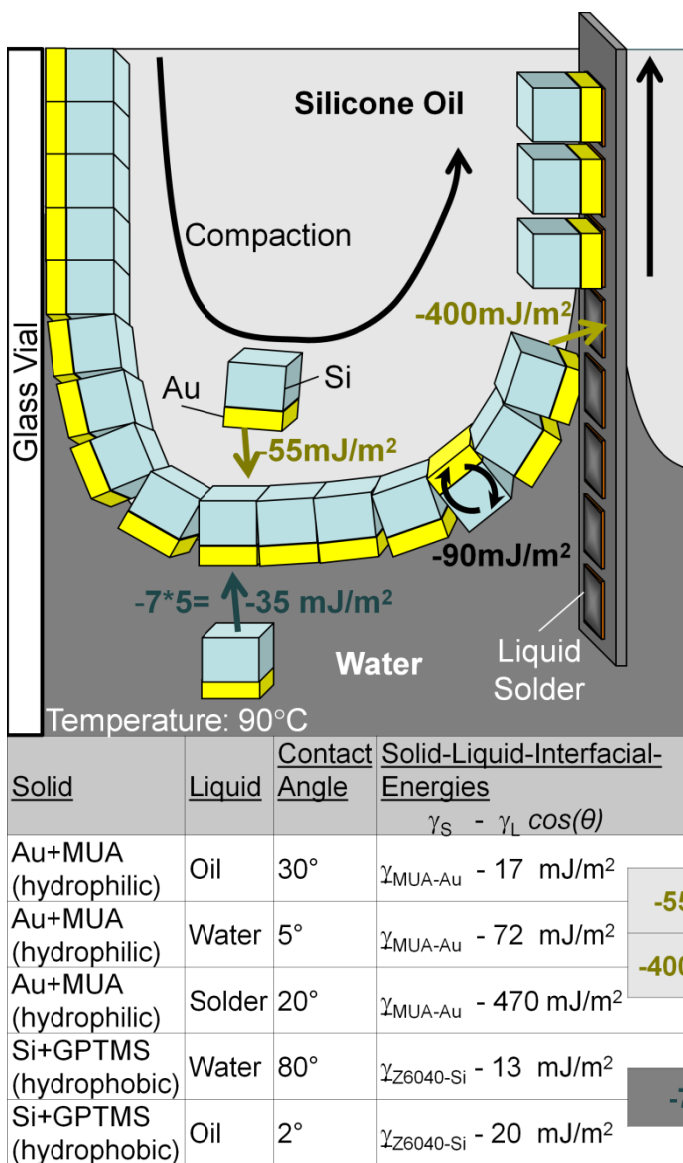
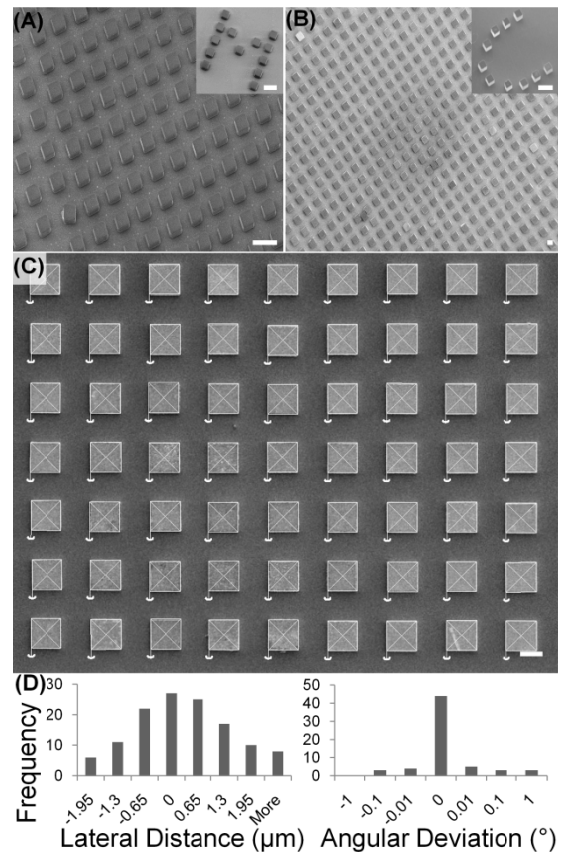


Figure 5 shows patterned self-assembly results of Si and SU-8 with 20  $\mu\text{m}$  and 60  $\mu\text{m}$  side lengths. Assembly with different area densities is tested using regular arrays ( $\sim 25\%$  area density; A,B) and arbitrary text ( $<5\%$  area density; A,B (insets)). Defects, measured by the cumulative number of missing, misaligned, and excess components, were found to be independent of the area density, component type, and component size. For example, Fig. 5A depicts 100 receptors carrying a single SU-8 component where one is misaligned reducing the yield to 99%. Fig. 3B depicts  $\sim 400$  receptors, each receptor carries a correctly aligned Si chiplet, however, three additional components were found to be present reducing the yield to 99.3%. These pictures are representative images of assemblies that extend over larger areas, currently limited to 1 cm long and wide substrates; the present assembly system has a 1  $\text{cm}^2$  interfacial area/capacity which provides room for  $\sim 250000$ ,  $20 \times 20 \mu\text{m}$  sized dies. The number of components that transfer onto the surface depends on the area covered by solder. For example, for the intermediate 25% area density test structures (A,B)  $\sim 62500$  components assemble onto the substrate in 45 seconds. Components assemble with good alignment accuracy which is determined using overlaid CAD measurement guides. For example, 60  $\mu\text{m}$  sized high precision Si components (C) yield an average placement accuracy of 0.9  $\mu\text{m}$  (STD) and angular orientation accuracy of 0.139 $^\circ$  (STD) (D).

**Fig. 5.** Scanning electron micrographs (SEMs) of (A) SU-8 (20  $\mu\text{m}$  side length) and (B, C) Si chiplets (20  $\mu\text{m}$  and 60  $\mu\text{m}$  side length) assembling in regular arrays and arbitrary text patterns (insets). The overlaid CAD guides visible in (C, white lines) are used to measure variations in the center-to-center distance and angular-orientation. (D) Histogram of measured variations. 40  $\mu\text{m}$  scale bars.

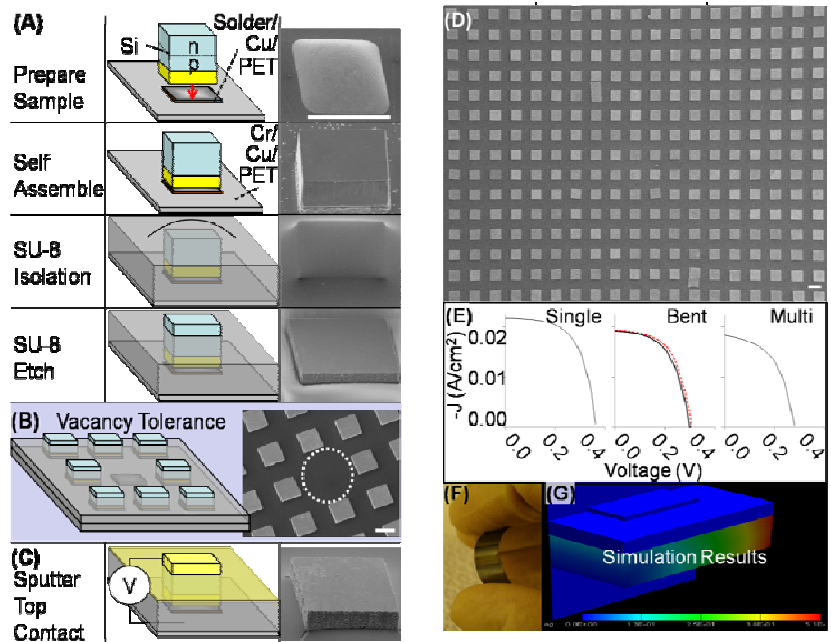


## VACANCY TOLERANT SEGMENTED FLEXIBLE MONTOCRYSTALLINE SOLAR CELL APPLICATION

A potential new application of fluidic self-assembly can be found in the manufacturing of solar cells on flexible substrates which could benefit from a reduction of material use and cost. Figure 6 illustrates the application of the process realizing a segmented monocrystalline solar cell on a flexible PET substrate reducing the material use of Si by a factor of 10 when compared to conventional monocrystalline cell architectures. The material reduction is achieved by using 20  $\mu\text{m}$  thin silicon chiplets instead of commonly used 200-300  $\mu\text{m}$  thick Si wafers where most of the Si is used to provide a mechanical support. The difference between the Si chiplets in this

figure and the Si chiplets used in previous test experiments is that they carry a p-n junction which is fabricated using a spin-on-dopant and a high temperature diffusion step before they are assembled onto the flexible PET substrate; the section on component fabrication provides further details. The process steps to form the solar cells (Fig. 6A) use an SU-8 isolation layer which is applied by spin coating before it is etched back in a reactive ion etcher to reveal the p-doped region of the chips. The section on component fabrication provides further details. The process is designed to be tolerant of assembly defects (Fig. 6B) where SU-8 fills in voids and locations of missing dies (vacancies); SU-8 and other polymers form a thinner film over protruding objects when compared to valleys when spun. This self-leveling behavior makes the cells tolerant against assembly defects; a missing Si diode (highlighted region, Fig. 6B) will not result in a short and failure of the cell since these regions are coated with SU-8. As a top contact we used a semitransparent 20 nm thin sputter deposited film of Au (Fig. 6C) and adjusted the input power accordingly, however, materials including transparent conducting oxides (TCOs) could be used as well. Figure 6D depicts a respective closeup (SEM) of the completed structure.

**Fig. 6.** Flexible segmented monocrystalline solar cell fabrication procedure, result, and characterization. (A) Assembly and isolation process next to scanning electron micrographs (SEM) representative of each step. (B) Defect tolerant design strategy and result (SEM) where vacancies are covered with SU-8 preventing shorts to the substrate. (C) Top contact deposition process and representative SEM. (D) Micrograph of an assembled array. (E) IV load curves of cells prior to assembly (left) and after assembly in unbend (red curve, center) and bent configuration (1cm radius of curvature, black curve, center); (E, right) IV load curve of a module as depicted in (F); (G) Finite element computer simulation of the strain inside the composite flexed (1cm radius of curvature) structure composed of a 175  $\mu$ m PET layer holding a 20  $\mu$ m thin film of Si cubes surrounded by SU-8 where the region of maximum strain is located at the top metal contact in the center between silicon cells. 60 $\mu$ m scale bars.



We tested the cells before and after assembly and found very little difference in terms of their electrical properties (Fig. 4E). Individual cells after they were released from the wafers had 4.4 % power conversion efficiencies, 0.34V open circuit voltage, and 0.67 filling factor at 0.7 suns (Philips PAR38 lamp, calibrated with an ILT 1400-A photometer) which could be improved to established levels by incorporating an intrinsic region and through optimization of doping levels/profiles, geometry, anti-reflection coatings, surface passivation layers, and contacts which is outside of the focus of this work. The cells retained the electrical properties (4.2% efficiency .30V, .56FF) (red line) confirming that the assembly procedure and exposure to the oil-water interface does not alter the cells. The electrical properties changed only slightly (3.8%,.31V,.55FF) (black line) when bent as long as the radius of curvature remains above 1 cm.



The change in the recorded I/V curve between bent and unbent structures is reversible suggesting that a change in the local illumination angle is the likely cause. We repeated the assembly of modules as shown in Fig. 4F several times and found a slight reduction in the open circuit voltage and short circuit current when compared to the original isolated cells. For example the module (marked as module 4) had an efficiency which was 1% smaller when compared with the original isolated cells (marked as isolated cell). This decrease in efficiency as the components are connected in parallel is likely due to variances in component doping, top contact uniformity, and isolation layer thicknesses. We have not yet tested effects of fatigue and minimal possible radius of curvature of bent structures but have observed situations where the top contact failed.

## CONCLUSIONS

In summary, we have demonstrated examples of the directed self-assembly of micrometer-sized components with single-angular orientation accuracy of  $0.3^\circ$  and contact-pad registration for  $280\mu\text{m} - 2\text{mm}$  sized dies. Alignment pedestals and registration to 7 contact pads has been shown providing a route to flip-chip self-assembly. Scaling down to 10-fold smaller chip dimensions, however, was not possible by a linear extension of the previous agitation concepts. Instead a new concept has been developed that makes use of a dynamic method that passes the chip through a liquid-liquid interface. This concept was applied to the assembly of monocrystalline silicon solar cell chiplets onto flexible and curved substrates.

## REFERENCES

- [1] M. B. Cohn, K. F. Bohringer, J. M. Noworolski, A. Singh, C. G. Keller, K. Y. Goldberg, R. T. Howe, *Proceedings of SPIE* **1998**, 3512, 2.
- [2] T. D. Clark, J. Tien, D. C. Duffy, K. E. Paul, G. M. Whitesides, *Journal of the American Chemical Society* **2001**, 123, 7677.
- [3] R. S. Fearing, *Proceedings* **1995**, 212.
- [4] S. Zhang, *Nature Biotechnology* **2003**, 21, 1171.
- [5] G. M. Whitesides, B. Grzybowski, *Science* **2002**, 295, 2418.
- [6] H. J. J. Yeh, J. S. Smith, *IEEE Photonics Technology Letters* **1994**, 6, 706.
- [7] J. S. Smith, H. J. J. Yeh, *US Patent* **1998**, 5,824,186.
- [8] D. H. Gracias, J. Tien, T. L. Breen, C. Hsu, E. M. Whitesides, *Science* **2000**, 289, 1170.
- [9] M. Boncheva, D. H. Gracias, H. O. Jacobs, G. M. Whitesides, *Proc. Natl. Acad. Sci. USA* **2002**, 99, 4937.
- [10] H. O. Jacobs, A. R. Tao, A. Schwartz, D. H. Gracias, G. M. Whitesides, *Science* **2002**, 296, 323.
- [11] U. Srinivasan, D. Liepmann, R. T. Howe, *Journal of Microelectromechanical Systems* **2001**, 10, 17.
- [12] U. Srinivasan, M. A. Helmbrecht, C. Rembe, R. S. Muller, R. T. Howe, *IEEE Journal of Selected Topics in Quantum Electronics* **2002**, 8, 4.
- [13] K. F. Böhringer, U. Srinivasan, R. T. Howe, Interlaken, Switzerland, **2001**.
- [14] W. Zheng, P. Buhlmann, H. O. Jacobs, *Proc. Natl. Acad. Sci. USA* **2004**, 101, 12814.
- [15] W. Zheng, H. O. Jacobs, *Applied Physics Letters* **2004**, 85, 3635.
- [16] W. Zheng, H. O. Jacobs, *Advanced Functional Materials* **2005**, 15, 732.
- [17] F. Patolsky, G. Zheng, C. M. Lieber, *Analytical Chemistry* **2006**, 78, 4260.
- [18] H. O. Jacobs, Z. Wei, USA, Provisional Application, **March 2006**.

- [19] C. R. Barry, H. O. Jacobs, *Nano Letters* **2006**, 6, 2790.
- [20] X. Xiong, Y. Hanein, J. Fang, Y. Wang, W. Wang, D. T. Schwartz, K. F. Bohringer, *Journal of Microelectromechanical Systems* **2003**, 12, 117.
- [21] S. A. Stauth, B. A. Parviz, *Proceedings of the National Academy of Sciences of the United States of America* **2006**, 103, 13922.
- [22] Robert J. Knuesel and Heiko O. Jacobs, *PNAS* **2010**, 107, 993. 